



Electrospray Plume Modeling for Rapid Life and Performance Analysis

Shehan M. Parmar,^{*} Adam L. Collins[†] and Richard E. Wirz[‡]
 University of California, Los Angeles, CA, 90095

A data-driven, reduced-order electrospray plume modeling framework has been developed to predict downstream mass flux evolution and thruster lifetime. The computational domain is the Plume Region, where charged plume species motion can be assumed to be governed solely by electrostatic forces. To enable a surrogate modeling approach, physics-based charged particle simulations were reduced to a single, analytical equation using polynomial chaos expansion (PCE) as the functional form. This model was then evaluated within a Bayesian inference framework using electrospray plume mass flux measurements taken at the UCLA Plasma & Space Propulsion Laboratory (PSPL). The unknown distribution in upstream input conditions for plume species emission angles was quantified with uncertainty bounds, showing the need for super-Gaussian-like distributions similar to downstream mass flux profiles. Model-predicted mass flux profiles indicate regions of higher uncertainty at wider angles, indicating the need for further experimental results at these locations.

I. Nomenclature

| | |
|------------------------------|--|
| \vec{E}_{ext} | = external electric field from electrospray electrodes |
| ϕ_{ext} | = potential field from electrospray electrodes |
| V_{jet} | = voltage at electrospray jet tip |
| $V_{emitter}$ | = voltage of electrospray emitter |
| ϕ_{ext} | = potential field from electrospray electrodes |
| θ_i | = initial line-of-sight angle of charged particle |
| θ_f | = final line-of-sight angle of charged particle |
| r_i | = initial radial position of charged particle |
| r_f | = final radial position of charged particle |
| z_i | = initial axial position of charged particle |
| z_f | = final axial position of charged particle |
| s_i | = initial speed of charged particle |
| s_f | = final speed of charged particle |
| γ_i | = initial emission angle of charged particle |
| γ_f | = final emission angle of charged particle |
| ρ | = propellant density |
| K | = propellant conductivity |
| Q | = flow rate |
| $\dot{m}(\theta)$ | = angular distribution of mass flux |
| $\dot{m}(\theta)_{loss}$ | = mass impingement on grids |
| θ_{crit} | = grid line-of-site angle |
| t_{sat} | = grid saturation time (i.e. electrospray end of life) |
| $\left(\frac{q}{m}\right)_i$ | = specific charge of charged particle i |
| S_i | = Sobol index for variable i |

^{*}PhD Student, UCLA Mechanical and Aerospace Engineering, 420 Westwood Plaza, Los Angeles, CA, and AIAA Student Member, parmar@ucla.edu

[†]Research Scientist, UCLA Mechanical and Aerospace Engineering, 420 Westwood Plaza, Los Angeles, CA, and AIAA Member, collinsalc55@ucla.edu

[‡]Professor, UCLA Mechanical and Aerospace Engineering, 420 Westwood Plaza, Los Angeles, CA, and AIAA Associate Fellow, wirz@ucla.edu

II. Introduction

Electrospray thrusters can achieve low thrust-noise ($\sim 100 \text{ nN} \cdot \text{Hz}^{-\frac{1}{2}}$) and high thrust-precision ($\sim \text{nN} - \mu\text{N}$) capabilities that enable future space missions such as the Laser Interferometer Space Antenna (LISA) and the Habitable Exoplanet Observatory (HabEx) [1–5]. Electrospays emit charged droplets by applying a strong electric field onto a highly-conductive ionic liquid to generate thrust. The primary challenge of modern electro spray technologies is the need for significant improvements in thruster lifetime to enable long-duration space missions. On board the recent LISA Pathfinder mission, the Colloid MicroNewton Thruster (CMNT) developed by Busek Co., Inc. and NASA Jet Propulsion Laboratory (JPL) demonstrated thruster lifetimes of approximately 2400 hours. Thus, there is a clear technological need for improved electro spray lifetime and performance in order to achieve nominal lifetime requirements of $\sim 40,000$ hours for the LISA mission, for instance [6].

To design electrospays that meet multi-year mission requirements, previous research has been dedicated to identifying the fundamental life-limiting failure mechanisms during thruster operation. In a hierarchical failure tree for electro spray life outlined by Thuppal et al. [7], overspray was considered the primary failure mechanism most influenced by thruster design considerations (e.g. operation and control, geometry, and material and propellant selection) [2, 7]. Overspray is defined as any emitted propellant directed towards the grids, or electrodes, of an electro spray, resulting in eventual saturation of the grids as well as induced secondary failure mechanisms including backspray and insulator wetting. Therefore, in order to effectively improve electro spray lifetime, it is critical to reduce any mass flux to the grids.

Consequently, accurate lifetime predictions require a better understanding of extraction and electro spray plume evolution mechanisms that influence mass flux to the grids. While previous retarding potential [8] and plume divergence angle [1] measurements have shown current density profiles of electro spray emission that follow Gaussian-like distributions, no evidence suggests that corresponding mass flux profiles follow the same distribution due to polydisperse plume profiles [7]. Recent characterization of electro spray plumes at the University of California, Los Angeles (UCLA) Plasma & Space Propulsion Laboratory (PSPL) have also shown dissimilar mass flux and current density profiles in shape and width highlighted by quartz crystal microbalance (QCM) measurements [9, 10]. Moreover, downstream plume profiles have an apparent, super-Gaussian functional form where massive species are detected out at high half-angles up to at least 40° . Resolving mass flux at such high angles becomes especially important since small deviations in plume profile shape can propagate into large uncertainties in expected lifetime.

To examine the underlying source of mass flux profiles observed experimentally, high-fidelity computational models are desired to ascertain the initial conditions that result in, for example, a super-Gaussian plume shape. It is known that the relevant physics-based phenomena for electro spray propulsion span multiple length and time scales: nanodroplet breakup [11] induced by ion evaporation [12–14] or Coulombic fission [15, 16], inter-droplet Coulomb interactions or space-charge [17–19], and cone-jet formation and extraction [20, 21]. Furthermore, secondary species emission (SSE) during droplet-mode electro spray operation must also be considered when validating models against measurements taken in vacuum test facilities [22]. To this end, the UCLA PSPL has discretized the electro spray computational domain into multiple regions, each modeled by their most dominant physics- or chemistry-based phenomena, as shown in Figure 1 [23].

The present study focuses on the Plume (or Exhaust) Region, where space charge effects can be considered negligible and plume evolution is dominated solely by applied electrostatic forces. The Propagation of Electro spray Plume Particles in the Exhaust Region (PEPPER) model serves as a reduced-order model capable of rapidly exploring the parameter space of interest. The PEPPER model is uniquely positioned in the computational domain to accept inputs from the Interaction Region, where the UCLA PSPL Discrete Electro spray Lagrangian Interaction (DELI) model can capture critical, inter-droplet Coulomb forces that result in negative velocity gradients among inhomogeneous charged droplet species [19]. The primary objective of this model is to determine the initial conditions that generate mass flux and current density plume profiles observed in previous studies by implementing a robust, data-driven framework. In this paper, the first section begins by outlining the proposed data-driven modeling framework involving a physics-based model that is captured by a computationally cheap surrogate or “metamodel” for efficient Bayesian inference analysis. In the second section, we provide results from both the physics-based and surrogate model that result in inferred emission-site input conditions for the UCLA PSPL electro spray thruster domain. The final section provides a discussion on the electro spray lifetime and performance implications learned from this framework.

III. Data-driven Modeling Methods

The PEPPER modeling framework employs reduced-order and surrogate techniques to decrease runtime and make use of Bayesian inference in lieu of high-fidelity, numerical simulations. By enabling both forward propagation

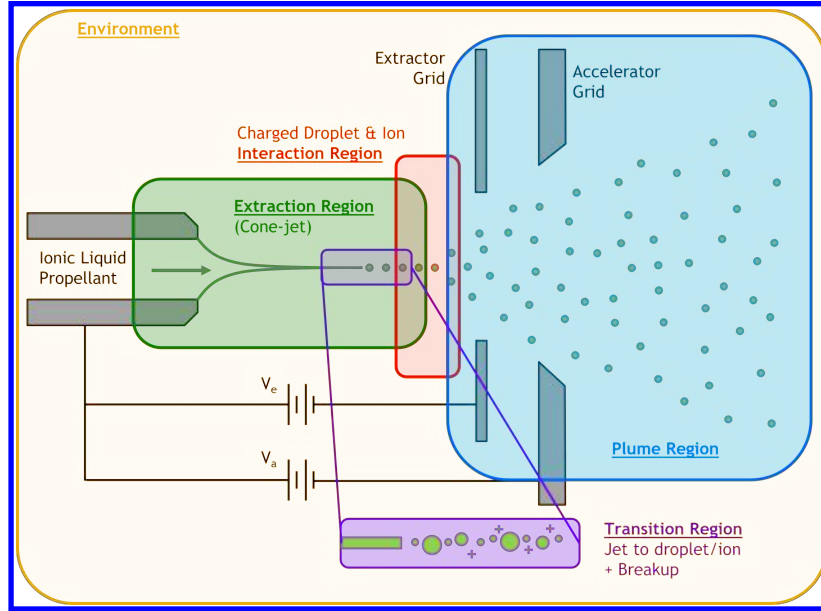


Fig. 1 UCLA PSPL Discretized Electrospray Computational Domain

of micro-scale outputs from higher-fidelity models and backward propagation using experimental measurements to inform likely input conditions, the PEPPER model will provide a means to quantify electrospray thruster lifetime and performance with minimal computational cost.

A. Plume Modeling Theory

As has been identified in high-fidelity plume models that include inter-droplet Coulomb interactions [17, 24], as charged particles escape the “critical” region or interaction region [19] a certain distance away from the emitter, the external electric field, \vec{E}_{ext} , generated by the electrodes dominates over Coulomb interactions. This enables the PEPPER model to greatly simplify the equations of motion within the Plume Region to

$$\frac{d^2 \vec{x}_i}{dt^2} = - \left(\frac{q}{m} \right)_i \nabla \phi_{ext} = \left(\frac{q}{m} \right)_i \vec{E}_{ext}, \quad (1)$$

where \vec{x}_i is the position of particle i , $\left(\frac{q}{m} \right)_i$ is the particle’s specific charge, and ϕ_{ext} is the potential field from the external boundary conditions at the emitter and extractor electrode. Figure 2 depicts a typical trajectory of a plume particle and the most pertinent variables. To solve for the final radial and axial positions, r_f and z_f , in the Plume Region, the particle’s initial emission characteristics must be known, namely the radial and axial positions, r_i and z_i , initial velocity magnitude and angle, s_i and γ_i , and species specific charge.

For the data-driven modeling task addressed in this study, the initial conditions needed to solve Equation 1 are considered unknown. This presents a challenge when estimating the initial distribution of $\left(\frac{q}{m} \right)_i$. While the disparity in mass flux and charge density profiles are indicative of non-uniform specific charge distributions, (i.e. $\frac{q}{m}(\theta)$), the mass flux profile measurements are obtained based on *all* massive species striking the QCM. Despite the lack of detailed resolution of species composition, an invariant property of charged particle motion can be invoked to reduce the unknown variables in this analysis. Concretely, for charged particles entering a domain with a constant, uniform electric field, any species with the same potential at the emission site, defined by the difference between the jet tip and emitter voltage,

$$V_{jet} - V_{emitter} = \frac{1}{2} \left(\frac{m}{q} \right)_i \vec{v}_i^2, \quad (2)$$

will follow the same trajectory. This is realized in the trivial case where the emission potential is set to zero, resulting in a straight line along the z -axis, irrespective of species specific charge; any subsequent perturbations to this

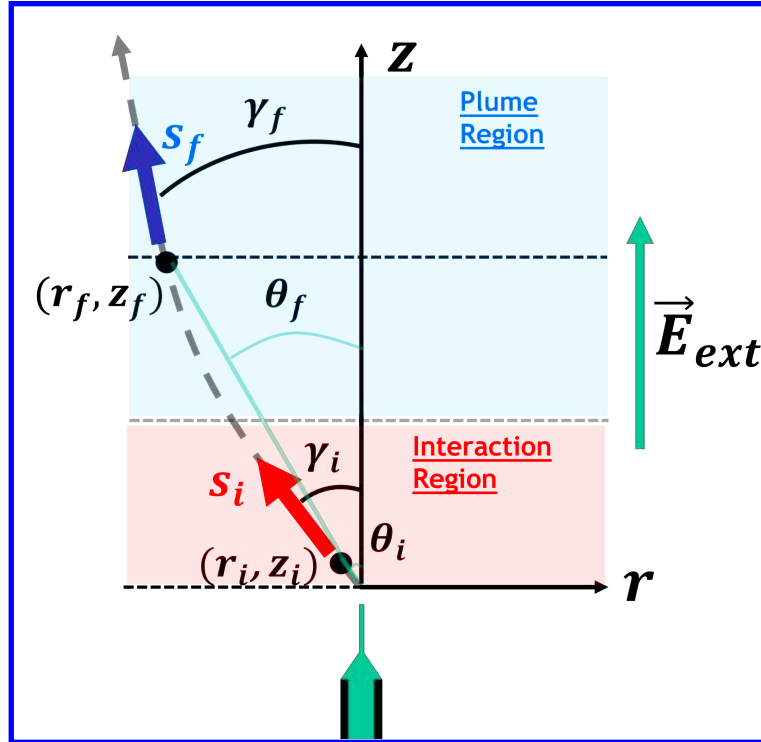


Fig. 2 Baseline trajectory of a typical particle starting from entering the Interaction Region at the emission site z_i , entering the Plume Region, and ultimately exiting a plane of interest at z_f . The trajectory is defined in terms of particle height z , speed s , direction γ , and line-of-sight angle θ .

value result in families of similar trajectory curves. Thus, particles initialized in the Plume Region domain are set with constant kinetic energy to charge ratios, where $\frac{1}{2} \left(\frac{m}{q} \right)_i s_i^2$ is estimated using inferred retarding potential analyzer (RPA) measurements for a specified flow rate Q , beam current I_B , and ionic liquid propellant, 1-ethyl-3-methylimidazolium bis(trifluoromethylsulfonyl) imide (EMI-Im) [25, 26]. Based on well-known scaling laws, Q and the propellant conductivity K can provide an estimated particle mass, shown in Equation 3,

$$m_i = \rho \frac{\pi}{6} \left(\frac{\varepsilon_0 Q}{K} \right), \quad (3)$$

where ρ is the propellant density, ε_0 is the vacuum permittivity, and droplet diameter is defined by $d = (\varepsilon_0 Q / K)^{\frac{1}{3}}$ [27]. It follows that the initial position θ_i and emission angle of the species γ_i are the remaining unknown variables to determine a plume particle trajectory. It is hypothesized that γ_i is the most relevant variable that controls overall radial plume expansion. The subsequent sections will outline the data-driven modeling framework used to infer the most probable initial distribution in $f(\gamma_i)$ based on experimental mass flux and current density profile measurements.

Based on an initial distribution of charged particles emitted into the Plume Region domain, the subsequent distribution of final positions in the form of $f(\theta_f)$ can be resolved for some defined downstream plane of interest, z_f . Using the analytical life model defined by Thuppl et al[7], the mass flux profile can be defined by Equation 4 [7],

$$\dot{m}(\theta_f) = \frac{Q\rho}{F_{full}} f(\theta_f), \text{ where } F_{full} = \int_0^\pi 2\pi \sin \theta f(\theta_f) d\theta. \quad (4)$$

The time it takes for the grids to be fully saturated to the point of failure, t_{sat} , is then defined by Equation 5

$$t_{sat} = \frac{\rho V_{crit}}{\dot{m}_{loss}}, \quad (5)$$

where V_{crit} is the accumulated propellant volume saturating the grid. The rate of mass impingement on the grid is defined by Equation 6,

$$\dot{m}_{loss} = 2\pi \int_{\theta_{crit}}^{\frac{\pi}{2}} \dot{m}(\theta_f) \sin \theta d\theta, \quad (6)$$

where θ_{crit} is the grid line-of-sight angle with respect to the emission site [7]. To perform this analysis, a computational model was built in the COMSOL Multiphysics software, version 5.6 to solve for the electric field and simulate charged particle trajectories.

B. Surrogate Model

As described above, the primary input parameters needed to solve for the particle's trajectory are the initial positions, θ_i , initial emission angles, γ_i , and the geometry-dependent variables, such as the $V_{electrode}$. If each of these input variables are assumed to be unknown, we would like to generate a computationally inexpensive method to explore a possibly large functional design space. Thus, a model surrogate, or "metamodel", defined by some arbitrary analytical function $Y = \mathbb{M}(\vec{X})$ can be defined to map the relevant inputs to the output of interest, as defined by Equation 7,

$$\mathbb{M} : \theta_i, \gamma_i, V_{electrode} \rightarrow \theta_f, \quad (7)$$

where (\vec{X}) denotes each of the input variables. In this case, the functional form of a polynomial chaos expansion (PCE) is selected to define the metamodel \mathbb{M} . PCEs have shown to be a suitable surrogate modeling technique for a wide range of engineering applications and robust data-driven workflows [28–30]. Its respective functional form is shown in Equation 8,

$$\mathbb{M}(\vec{X}) = \sum_{\alpha \in \mathbb{N}^d} y_{\alpha} \Psi_{\alpha}(\vec{X}), \quad (8)$$

where a basis set of multivariate, orthogonal polynomials, $\{\Psi_{\alpha}(\vec{X}), \alpha \in \mathbb{N}^d\}$, is bounded by the dimension d of the input parameter space \vec{X} . Each polynomial, or "mode", is weighted by coefficient y_{α} to generate the entire PCE function. The coefficients y_{α} are determined using a standard regression procedure by first obtaining results from the physics-based computational model (i.e. charged particle tracing in COMSOL). For the following analysis, the input parameter space is sampled using well-known quasi-random sampling techniques, such as Latin hypercube or Sobol methods [31]. Both sampling and regression methods are implemented using an open-source Python package, Chaospy [32]. The resulting model surrogate resolves the final position of the particle using a single analytical equation.

C. Bayesian Inference

The mapping introduced in Equation 7 enables rapid evaluation of arbitrary distributions in each of the individual variables. In order to determine the unknown variables, a Bayesian inference approach becomes a suitable method of analysis. The goal of Bayesian inference is to generate a posterior distribution for a series of hypotheses [33]. Bayes' theorem is comprised of two terms, the likelihood function and prior distribution, shown in the right-hand side of Equation 9

$$\text{prob}(\theta_i, \gamma_i | \dot{m}(\theta)_{UCLA, QCM}, I) \propto \text{prob}(\dot{m}(\theta)_{UCLA, QCM} | \theta_i, \gamma_i, I) \cdot \text{prob}(\theta_i, \gamma_i | I), \quad (9)$$

where θ_i and γ_i are the uncertain parameters, or hypotheses, we wish to quantify (assuming some constant $V_{electrode}$), $\dot{m}(\theta)_{UCLA, QCM}$ denotes the available mass flux profile measurements provided by UCLA PSPL QCM results, and I represents any background knowledge available for this problem. The posterior distribution is solved by implementing a Hamiltonian Monte Carlo (HMC) No U-Turn Sampling technique using an open-source Bayesian inference Python tool, PyMC3 [34]. In this way, the unknown variables can be directly quantified and bounded by uncertainty envelopes to determine a set of initial conditions near the site of electrospray emission that lead to the experimentally observed, super-Gaussian mass flux profiles [10].

IV. Results

A. Physics-based and Surrogate Model

Charged particle trajectories are solved using the COMSOL Multiphysics Electric Field Solver and Charged Particle Tracing module. The potential field is shown in Figure 3 for an electrospray domain representative of the experimental

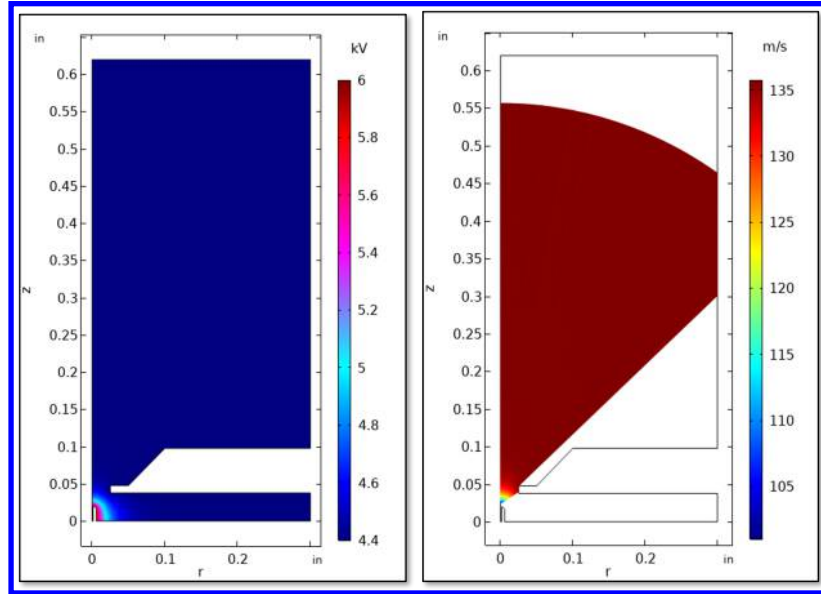


Fig. 3 Potential field solution (left) of electro spray geometry with an extractor electrode and particle trajectory sweep (right) over representative γ_i values.

conditions at the UCLA PSPL.

Figure 3 illustrates the plume particle trajectories using an initial parameter sweep over representative values for γ_i . Initial conditions for the kinetic energy to charge ratio were set to be on the order of ~ 1000 V to match experimental RPA results for droplet-mode electro spray emission using EMI-Im propellant [25, 26].

Initial positions, emission angles, and electrode voltages were sampled to generate the PCE according to Equation 8. The resulting PCE has the unique property of being a square-integrable function, first noted by Sudret [35, 36], such that total variance of a PCE as well as the partial variance contributions from each independent input variable can be evaluated using the Analysis Of Variance (ANOVA) decomposition technique. By normalizing the partial variance V_u by the total variance V_T , the Sobol index is derived, shown in Equation 10 [37]

$$S_i = \frac{V_u}{V_T}, \text{ where } \sum_{i=1} S_i = 1. \quad (10)$$

The Sobol index can be used to illustrate a model's sensitivity to a set of input parameters based on some single output. For the case of the PEPPER model, the resulting Sobol indices are shown in Figure 4, where the chosen output was selected to be the final line-of-sight position, θ_f , of the Plume Region particle based on Equation 7. Figure 4 confirms the original hypothesis that the initial emission angle is the most critical parameter based on the assumptions made by this model. That is, the final positions of Plume Region particles (and subsequently, the mass flux profile) is most influenced by changes in γ_i , which can easily perturb how narrow or far out wide a particle is emitted into the domain.

B. Bayesian Inference

Following Equation 9, a likelihood function was selected based on the functional form of experimental observations (i.e. Gaussian to super-Gaussian),

$$\text{prob}(\dot{m}(\theta)_{UCLA,QCM} | \theta_i, \gamma_i, I) = \prod_i^N \text{prob}(\dot{m}(\theta)_i | \theta_i, \gamma_i, I) \quad (11)$$

where the $\dot{m}(\theta)_i$ is estimated by applying $f(\theta_f) = \mathbb{M}(f(\gamma_i), \theta_i = 0, V_{electrode} = 4.4kV)$ to Equation 4. The unknown parameters are found in the distribution of emission angles,

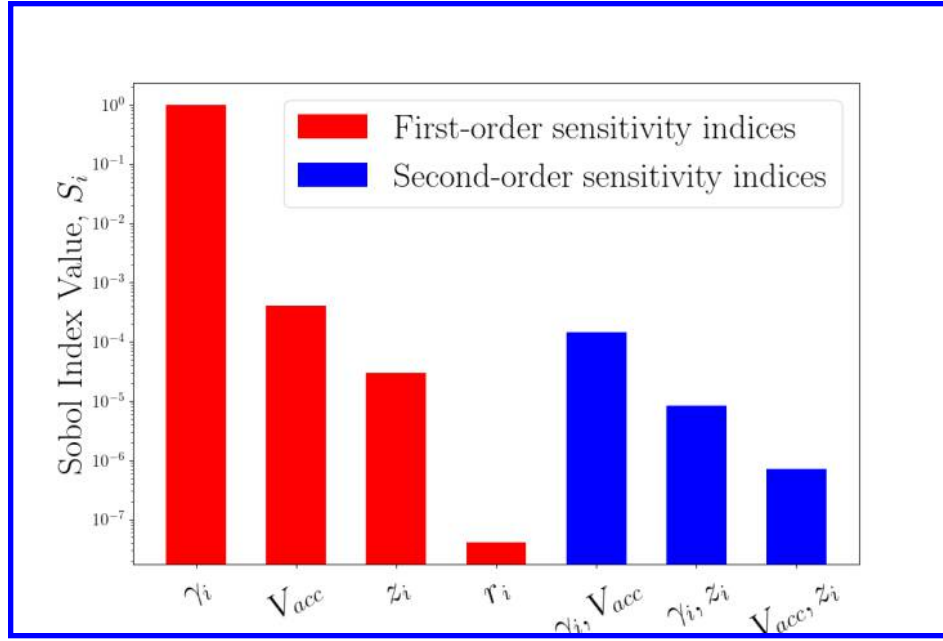


Fig. 4 First and second-order sensitivity analysis using variance-based Sobol indices for PEPPER model parameters.

$$f(\gamma_i) = A \exp\left(-\left(\frac{(\gamma - \mu)^2}{2\sigma^2}\right)^n\right). \quad (12)$$

Thus, the likelihood function preserves physically-informed unknown parameters that describe a plume profile at any location downstream of the emission site, including the profile amplitude, A , width, σ , tilt, μ , and sharpness, n . The prior distributions were selected as normal distributions and are shown for each variable in Equation 13:

$$A_1 \sim \mathcal{N}(200, 100); \mu_1 \sim \mathcal{N}(0, 10^{-3}); \sigma_1 \sim \mathcal{N}(100, 50); n_1 \sim \mathcal{N}(1.5, 1). \quad (13)$$

After taking 1500 HMC samples, the resulting posterior distributions are shown in Figure 5 along with the corresponding trace plots. A trace plot shows the parameter values over every iteration and serves as a diagnostic to detect any divergences or outliers. In this case, all sampled data points lie within the same orders-of-magnitude and show no non-physical parameter values.

Figure 5 can then be used to show the resulting emission angle distribution defined in Equation 12, shown in Figure 6. This plot provides the shape and form of the initial distribution in emission angles that match with the experimental data. If we propagate out the initial distribution from Figure 6 using the surrogate model, \mathbb{M}_{PCE} , then we get $\hat{m}(\theta)$ that is also shown on Figure 6.

V. Discussion

The model discussed above successfully establishes a complete, data-driven framework by using mass flux measurements at the UCLA PSPL to elucidate unknown physical-parameters relevant for characterizing emission behavior. The resulting posterior distributions were provided with trace plots that indicate an appropriately chosen prior distribution since no divergences or non-physical parameter values resulted when solving for Equation 9. The posterior distributions in Figure 5 resulted in predicted mass flux profiles showing 94% confidence envelopes. However, the data point near the tail of the mass flux distribution in Figure 6 is not captured by the model. Furthermore, it is apparent that the super-Gaussian nature of the downstream profiles is preserved in the initial conditions. In other words, super-Gaussian behavior of electrostatically-dominated particle motion near the emission site is necessary for generating super-Gaussian profiles further downstream.

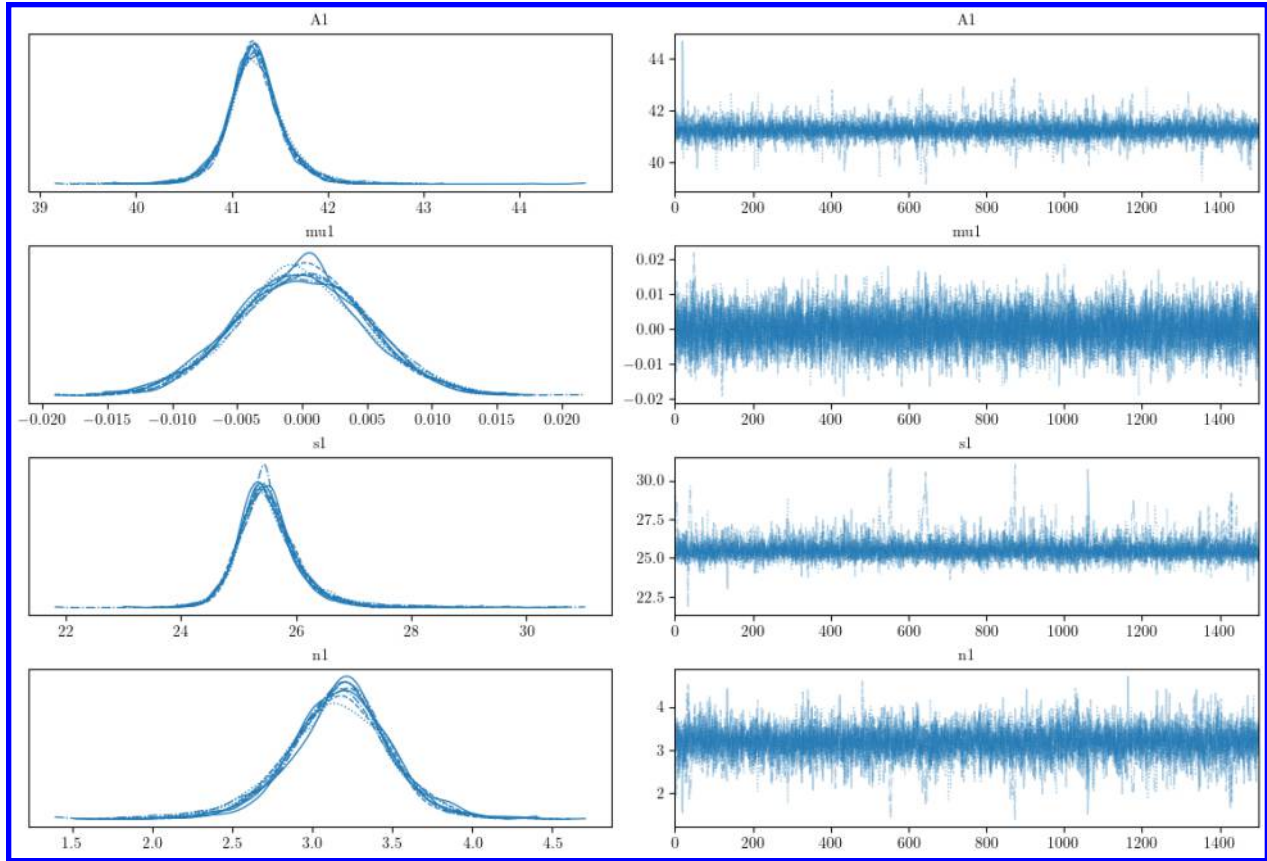


Fig. 5 Posterior distributions (left) for unknown parameters in emission angle distribution, including amplitude, A_1 , tilt, μ_1 , width, σ_1 , and sharpness n_1 (left) and trace plot (right) for each sampled maximum likelihood parameter value. Included plots were visualized using ArviZ [38].

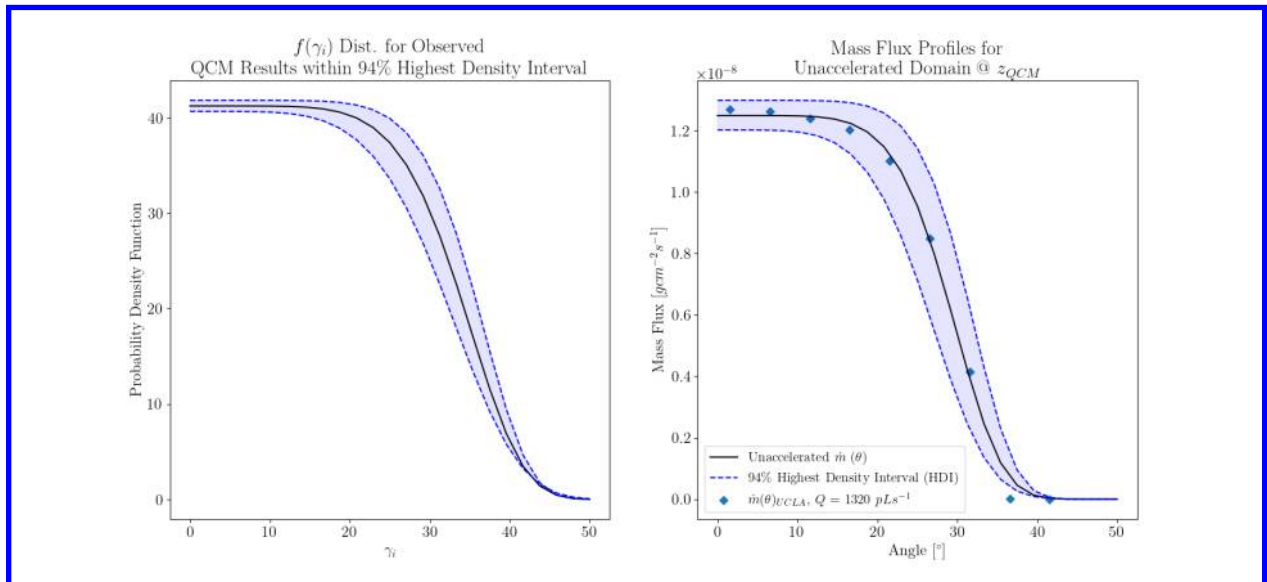


Fig. 6 Initial emission angle distribution, $f(\gamma_i)$, at emission site (left) and comparison between model predictions and experimental observations (right).

A. Implications on Acquiring New Data

In Section IV, we found that the relative uncertainty in mass flux was greatest at higher angles of the plume profile. Lifetime calculations depend heavily on the integrated mass flux wherever the grids are located. This region of low confidence indicates that more data are required to further confine the posterior probability distributions at high angles and obtain more accurate modeling results. Moreover, as was mentioned in the introduction section, the polydispersity of the plume is unknown and greater details regarding the evolved species downstream are desirable. Moreover, in order to predict thrust, neutrally-charged particles also need to be identified.

B. Implications on Improving Model Fidelity

In Section IV, we also find that based on the PEPPER model's primary assumptions that particles are governed solely by the external electric field, the super-Gaussian plumes that evolve downstream must have an underlying super-Gaussian emission angle profile to begin with. Limited theoretical backing for initial generation of a super-Gaussian plume suggests that additional terms may be necessary in the equations of motion to describe emission characteristics. For instance, the source of nonlinear inter-particle interactions and collisions may contribute to the non-Gaussian behavior of the *upstream* plume. In this regard, in subsequent iterations of the proposed data-driven model, Coulomb interactions, ion evaporation, and fission physics may be necessary terms to include in the overall model. Neighboring models, such as the DELI model, can thus be utilized to increase fidelity of the physics-based simulations established in this framework. The benefit of the reduced-order model presented in this study is to simplify the complexity of the problem and inform the optimal path forward (i.e. obtain more data at high angles, add Coulomb interaction terms, and so on).

VI. Conclusions

In this work, the Propagation of Electrospray Plume Particles in the Exhaust Region (PEPPER) model was developed to investigate mass flux evolution in an electrospray plume. The reduced-order, data-driven framework exploits the simplified physics-based approximations that can be made in the Plume Region, where particle trajectories are governed solely by electrostatic forces imposed by the electrodes. The computational complexity of the model was further reduced by resolving coefficients of a polynomial chaos expansion, enabling the use of a model surrogate during Bayesian inference analysis. The results indicate that in order to generate super-Gaussian profiles far downstream, an initial super-Gaussian-like distribution in emission angles of particles entering the electrostatically-dominated Plume Region is likely. The results also suggest that more experimental data in low-confidence regions (i.e. at high plume angles) and more information regarding species distribution will further improve confining posterior distributions of the model outputs. Future versions of PEPPER are under development for comparing charge and mass flux profiles as well as comparing accelerated and unaccelerated plumes.

VII. Acknowledgements

The authors thank Colleen Marrese-Reading, Steven Arestie, and John Ziemer from NASA JPL and Nathaniel Demmons of Busek Co. Inc. for their insightful discussions. The authors also thank Ani Thupput, McKenna Davis Breddan, Henry Huh, Nolan Uchizono, and Peter Wright for their insightful discussions. This material is based upon work supported by the U.S. Department of Energy, Office of Science, Office of Advanced Scientific Computing Research, Department of Energy Computational Science Graduate Fellowship under Award Number DE-SC0022158. This work was also funded by NASA/JPL Award No. 1580267 and Air Force Office of Scientific Research Award No. FA9550-21-1-0067.

References

- [1] Hruby, V., Spence, D., Demmons, N., Roy, T., Ehrbar, E., Zwahlen, J., Martin, R., Ziemer, J., Connolly, W., Rhodes, S., and Tolman, W., "ST7-DRS Colloid Thruster System Development and Performance Summary," *44th AIAA/ASME/SAE/ASEE Joint Propulsion Conference & Exhibit*, Joint Propulsion Conferences, American Institute of Aeronautics and Astronautics, 2008. <https://doi.org/doi:10.2514/6.2008-4824>, URL <https://doi.org/10.2514/6.2008-4824>.
- [2] Ziemer, J. K., "Performance of Electrospray Thrusters," *31st International Electric Propulsion Conference*, Ann Arbor, MI, USA, 2009, p. pp. 1–13.
- [3] Racca, G. D., and McNamara, P. W., "The LISA Pathfinder Mission," *Space Science Reviews*, Vol. 151, No. 1, 2010, pp. 159–181. <https://doi.org/10.1007/s11214-009-9602-x>, URL <https://doi.org/10.1007/s11214-009-9602-x>.

- [4] Demmons, N. R., Lamarre, N., Ziemer, J. K., Parker, M., and Spence, D., "Electrospray Thruster Propellant Feedsystem for a Gravity Wave Observatory Mission," *52nd AIAA/SAE/ASEE Joint Propulsion Conference*, AIAA Propulsion and Energy Forum, American Institute of Aeronautics and Astronautics, 2016. <https://doi.org/doi:10.2514/6.2016-4739>, URL <https://doi.org/10.2514/6.2016-4739>.
- [5] Mennesson, B., "Habitable Exoplanet Observatory Final Report," Tech. rep., NASA Jet Propulsion Laboratory, NASA Jet Propulsion Laboratory, Pasadena, California, 2019.
- [6] Amaro-Seoane, P., Audley, H., Babak, S., Baker, J. M., Barausse, E., Bender, P. L., Berti, E., Binétruy, P., Born, M., Bortoluzzi, D., Camp, J. B., Caprini, C., Cardoso, V., Colpi, M., Conklin, J. W., Cornish, N. J., Cutler, C., Danzmann, K., Dolesi, R., Ferraioli, L., Ferroni, V., Fitzsimons, E. D., Gair, J. R., Boté, L. G., Giardini, D., Gibert, F., Grimaldi, C., Halloin, H., Heinzel, G., Hertog, T., Hewitson, M., Holley-Bockelmann, K., Hollington, D., Hueller, M., Inchauspe, H., Jetzer, P., Karnesis, N., Killow, C. J., Klein, A., Klipstein, B., Korsakova, N. K., Larson, S. L., Livas, J. C., Lloro, I., Man, N., Mance, D., Martino, J., Mateos, I., Mckenzie, K., McWilliams, S. T., Miller, C., Mueller, G., Nardini, G., Nelemans, G. A., Nofrarias, M., Petiteau, A., Pivato, P., Plagnol, E., Porter, E. K., Reiche, J., Robertson, D. L., Robertson, N. A., Rossi, E. M., Russano, G., Schutz, B. F., Sesana, A., Shoemaker, D. P., Slutsky, J., Sopuerta, C. F., Sumner, T. J., Tamanini, N., Thorpe, I. J., Troebs, M., Vallisneri, M., Vecchio, A., Vetrugno, D., Vitale, S., Volonteri, M., Wanner, G., Ward, H., Wass, P. J., Weber, W. J., Ziemer, J. K., and Zweifel, P., "Laser Interferometer Space Antenna," Tech. rep., 2012.
- [7] Thuppal, A., Wright, P. L., Collins, A. L., Ziemer, J. K., and Wirz, R. E., "Lifetime Considerations for Electrospray Thrusters," *Aerospace*, Vol. 7, No. 8, 2020. <https://doi.org/10.3390/aerospace7080108>.
- [8] Gamero-Castaño, M., "Characterization of the electrosprays of 1-ethyl-3-methylimidazolium bis(trifluoromethylsulfonyl) imide in vacuum," *Physics of Fluids*, Vol. 20, No. 3, 2008. <https://doi.org/10.1063/1.2899658>.
- [9] Thuppal, A., Collins, A. L., Wright, P. L., Uchizono, M., Nolan, and Wirz, R. E., "Spatially-Resolved Mass Flux and Current Measurements of Electrospray Plumes," *36th International Electric Propulsion Conference*, Vienna, Austria, 2019.
- [10] Thuppal, A., Collins, A. L., Wright, P. L., Uchizono, N. M., and Wirz, R. E., "Mass flux and current density distributions of electrospray plumes," *Journal of Applied Physics*, Vol. 130, No. 10, 2021, p. 103301. <https://doi.org/10.1063/5.0056761>, URL <https://doi.org/10.1063/5.0056761>.
- [11] Prince, B. D., Tirupathi, P., Bemish, R. J., Chiu, Y.-H., and Maginn, E. J., "Molecular Dynamics Simulations of 1-Ethyl-3-methylimidazolium Bis[(trifluoromethyl)sulfonyl]imide Clusters and Nanodrops," *The Journal of Physical Chemistry A*, Vol. 119, No. 2, 2015, pp. 352–368. <https://doi.org/10.1021/jp507073e>, URL <https://doi.org/10.1021/jp507073e>.
- [12] Iribarne, J. V., and Thomson, B. A., "On the evaporation of small ions from charged droplets," *The Journal of Chemical Physics*, Vol. 64, No. 6, 1976, pp. 2287–2294. <https://doi.org/10.1063/1.432536>, URL <https://aip.scitation.org/doi/abs/10.1063/1.432536>.
- [13] Gamero-Castaño, M., "Electric-Field-Induced Ion Evaporation from Dielectric Liquid," *Physical Review Letters*, Vol. 89, No. 14, 2002, p. 147602. <https://doi.org/10.1103/PhysRevLett.89.147602>, URL <https://link.aps.org/doi/10.1103/PhysRevLett.89.147602>.
- [14] Coffman, C., "Electrically-Assisted Evaporation of Charged Fluids: Fundamental Modeling and Studies on Ionic Liquids," Ph.D. thesis, Massachusetts Institute of Technology, 2016. URL <http://dspace.mit.edu/handle/1721.1/7582>.
- [15] Gu, W., Heil, P. E., Choi, H., and Kim, K., "Comprehensive model for fine Coulomb fission of liquid droplets charged to Rayleigh limit," *Applied Physics Letters*, Vol. 91, No. 6, 2007, p. 64104. <https://doi.org/10.1063/1.2767774>, URL <https://doi.org/10.1063/1.2767774>.
- [16] Hekmat, M. H., Rahmanpour, M., Mahmoudi, M., and Saharkhiz, S., "A genetic algorithm-based approach for numerical solution of droplet status after Coulomb fission using the energy conservation method," *Journal of Computational Applied Mechanics*, Vol. 51, No. 2, 2020, pp. 454–463. <https://doi.org/10.22059/JCAMECH.2020.304872.523>.
- [17] Deng, W., and Gomez, A., "Influence of space charge on the scale-up of multiplexed electrosprays," *Journal of Aerosol Science*, Vol. 38, No. 10, 2007, pp. 1062–1078. <https://doi.org/https://doi.org/10.1016/j.jaerosci.2007.08.005>, URL <http://www.sciencedirect.com/science/article/pii/S0021850207001358>.
- [18] Grifoll, J., and Rosell-Llompart, J., "Efficient Lagrangian simulation of electrospray droplets dynamics," *Journal of Aerosol Science*, Vol. 47, 2012, pp. 78–93. <https://doi.org/10.1016/j.jaerosci.2012.01.001>, URL <http://dx.doi.org/10.1016/j.jaerosci.2012.01.001>.
- [19] Davis, M. J., Collins, A. L., and Wirz, R. E., "Electrospray Plume Evolution Via Discrete Simulations," *36th International Electric Propulsion Conference*, Vienna, Austria, 2019.

- [20] Gamero-Castaño, M., “Energy dissipation in electrosprays and the geometric scaling of the transition region of cone–jets,” *Journal of Fluid Mechanics*, Vol. 662, 2010, pp. 493–513. <https://doi.org/DOI:10.1017/S0022112010003423>, URL <https://www.cambridge.org/core/article/energy-dissipation-in-electrosprays-and-the-geometric-scaling-of-the-transition-region-of-conejets/7CFA007BFDD4A06EC20F6F9BFF04D80F>.
- [21] Huh, H., and Wirz, R., “Numerical Simulation of Electrospray Thruster Extraction,” *36th International Electric Propulsion Conference*, Vienna, Austria, 2019.
- [22] Uchizono, N. M., Collins, A. L., Marrese-Reading, C., Arestie, S. M., Ziemer, J. K., and Wirz, R. E., “The role of secondary species emission in vacuum facility effects for electrospray thrusters,” *Journal of Applied Physics*, Vol. 130, No. 14, 2021. <https://doi.org/10.1063/5.0063476>.
- [23] Wirz, R. E., Collins, A. L., Thuppul, A., Wright, P. L., Uchizono, N. M., Huh, H., Davis, M. J., Ziemer, J. K., and Demmons, N. R., “Electrospray Thruster Performance and Lifetime Investigation for the LISA Mission,” *AIAA Propulsion and Energy 2019 Forum*, AIAA Propulsion and Energy Forum, American Institute of Aeronautics and Astronautics, 2019. <https://doi.org/doi:10.2514/6.2019-3816>, URL <https://doi.org/10.2514/6.2019-3816>.
- [24] Gamero-Castaño, M., “Characterization and modeling of colloid thruster beams,” *Collection of Technical Papers - AIAA/ASME/SAE/ASEE 42nd Joint Propulsion Conference*, Vol. 4, No. July, 2006, pp. 3256–3261. <https://doi.org/10.2514/6.2006-4643>.
- [25] Gamero-Castaño, M., “Characterization of the electrosprays of 1-ethyl-3-methylimidazolium bis(trifluoromethylsulfonyl) imide in vacuum,” *Physics of Fluids*, Vol. 20, No. 3, 2008, p. 32103. <https://doi.org/10.1063/1.2899658>, URL <https://doi.org/10.1063/1.2899658>.
- [26] Gamero-Castaño, M., and Cisqueira-Serra, A., “Electrosprays of highly conducting liquids: A study of droplet and ion emission based on retarding potential and time-of-flight spectrometry,” *Physical Review Fluids*, Vol. 6, No. 1, 2021, pp. 1–20. <https://doi.org/10.1103/physrevfluids.6.013701>.
- [27] GAÑÁN-CALVO, A. M., “On the general scaling theory for electrospraying,” *Journal of Fluid Mechanics*, Vol. 507, 2004, pp. 203–212. <https://doi.org/DOI:10.1017/S0022112004008870>, URL <https://www.cambridge.org/core/article/on-the-general-scaling-theory-for-electrospraying/32BA3083193B3B246663D07516F6E0E8>.
- [28] Kerr, D., “Sensitivity Analysis and Uncertainty Quantification in Reduced-Order Monopropellant Catalyst Bed Model,” Ph.D. thesis, University of California, Los Angeles, 2019.
- [29] Shen, D., Wu, H., Xia, B., and Gan, D., “Polynomial Chaos Expansion for Parametric Problems in Engineering Systems: A Review,” *IEEE Systems Journal*, Vol. 14, No. 3, 2020, pp. 4500–4514. <https://doi.org/10.1109/JSYST.2019.2957664>.
- [30] Acar, E., Bayrak, G., Jung, Y., Lee, I., Ramu, P., and Ravichandran, S. S., “Modeling, analysis, and optimization under uncertainties: a review,” *Structural and Multidisciplinary Optimization*, 2021. <https://doi.org/10.1007/s00158-021-03026-7>, URL <https://doi.org/10.1007/s00158-021-03026-7>.
- [31] Hadigol, M., and Doostan, A., “Least squares polynomial chaos expansion: A review of sampling strategies,” *Computer Methods in Applied Mechanics and Engineering*, Vol. 332, 2018, pp. 382–407. <https://doi.org/https://doi.org/10.1016/j.cma.2017.12.019>, URL <https://www.sciencedirect.com/science/article/pii/S0045782517307697>.
- [32] Feinberg, J., and Langtangen, H. P., “Chaospy: An open source tool for designing methods of uncertainty quantification,” *Journal of Computational Science*, Vol. 11, 2015, pp. 46–57. <https://doi.org/https://doi.org/10.1016/j.jocs.2015.08.008>, URL <https://www.sciencedirect.com/science/article/pii/S187750315300119>.
- [33] Sivia, D. S., and Skilling, J. J., *Data analysis a Bayesian tutorial*, 2nd ed., Oxford University Press, Oxford, 2006.
- [34] Salvatier, J., Wiecki, T. V., and Fonnesbeck, C., “Probabilistic programming in Python using PyMC3,” *PeerJ Computer Science*, Vol. 2, 2016, p. e55. <https://doi.org/10.7717/peerj-cs.55>, URL <https://doi.org/10.7717/peerj-cs.55>.
- [35] Sudret, B., “Global sensitivity analysis using polynomial chaos expansions,” *Reliability Engineering & System Safety*, Vol. 93, No. 7, 2008, pp. 964–979. <https://doi.org/https://doi.org/10.1016/j.ress.2007.04.002>, URL <https://www.sciencedirect.com/science/article/pii/S0951832007001329>.
- [36] Sobol, I. M., “Global sensitivity indices for nonlinear mathematical models and their Monte Carlo estimates,” *Mathematics and Computers in Simulation*, Vol. 55, No. 1-3, 2001, pp. 271–280. [https://doi.org/10.1016/S0378-4754\(00\)00270-6](https://doi.org/10.1016/S0378-4754(00)00270-6).
- [37] Sobol, I. M., “Sensitivity Estimates for Nonlinear Mathematical Models,” , 1993.
- [38] Martín, R. K., Carroll, C., Hartikainen, A., and Osvaldo, “ArviZ: a unified library for exploratory analysis of Bayesian models in Python,” *Journal of Open Source Software*, Vol. 4, No. 33, 2019, p. 1143. <https://doi.org/10.21105/joss.01143>.